International Journal of Automotive Technology, Vol. 18, No. 5, pp. 759−768 (2017)
DOI 10.1007/s12239−017−0075−8

pISSN 1229−9138/ eISSN 1976−3832

NUMERICAL STUDY OF THE EARLY INJECTION PARAMETERS ON WALL WETTING CHARACTERISTICS OF AN HCCI DIESEL ENGINE USING EARLY INJECTION STRATEGY

Hanzhengnan Yu, Xingyu Liang* and Gequn Shu

State Key Laboratory of Engines, Tianjin University, Tianjin 300072, China

(Received 4 October 2016; Revised 16 January 2017; Accepted 27 February 2017)

ABSTRACT−Wall wetting in the early injection period has been proved to be unavoidable in the HCCI (Homogeneous charge compression ignition) diesel engine using early injection strategy, which directly affects in-cylinder fuel-air mixture formation. In this study, the effects of the early injection parameters (injection timing, injection angle and injection pressure) on wall wetting characteristics of an HCCI diesel engine using early injection strategy have been numerically investigated. The variations of maximum wall film mass, evaporated wall film mass and residual wall film mass have been summarized. The concept of MHI (Mixture Homogenous Index) is introduced to evaluate the homogeneity of fuel-air mixture in the wall wetting region. In additions, the effects of the early injection parameters on the HC (Hydrocarbon Compounds) and CO (Carbon Monoxide) emissions have also been discussed. Results showed that in order to decrease the HC and CO emission caused by wall wetting as low as possible, it was better to increase the injection pressure and to advance the injection timing. The most effective method was to narrow the injection angle, In addition, the impingement target should be considered for choosing the injection timing and injection angle, and the impingement target of the piston bowl lip was recommended due to the enhancement of the atomization and the higher surface temperature.

KEY WORDS : Computational Fluid Dynamics (CFD), Early injection parameters, Wall wetting characteristics, Mixture formation, Emissions

1. INTRODUCTION

To solve the NOx and soot trade-off problem of the conventional diesel, a number of advanced combustion technologies have been studied (Yao *et al*., 2009; Kook *et al*., 2007; Berggren and Magnusson, 2012; Musculus *et al*., 2013). Homogeneous charge compression ignition (HCCI) combustion is one of the technologies, which was first proposed by Onishi *et al*. (1979) and Noguchi *et al*. (1979). The main characteristic for HCCI is a (more or less homogeneous) premixed fuel-air mixture that undergoes auto-ignition as a result of compression. However, one of critical challenges for HCCI is to obtain a homogeneous fuel-air mixture. This is especially true for diesel engines, as the lower volatility of diesel fuels makes it more difficult to form a homogeneous mixture than the gasoline fuels.

In order to obtain enough time for fuel to mix with the air before combustion, the early injection strategy by which the fuel is injected in an early stage of the compression stroke has been utilized widely in HCCI diesel engines.

However, because of the lower gas temperature and density at the early injection timing, some fuel spray unavoidablyimpinges with the cylinder wall or piston head and forms wall film (Kitasei *et al*., 2008; Benajes *et al*., 2012), which is called wall wetting. Due to the unavoidable occurrence of wall wetting, over rich fuel-air mixture is developed in the near wall region and leads the incomplete combustion which is a major reason for excessive HC and CO emissions. Moreover, the wall film formed on the cylinder wall also have a dilution effect on the lubricating oil, which will shorten its service life (Jia *et al*., 2008; Zhang *et al*., 2014; Yu *et al*., 2015).

Many researchers investigated the effect of the early injection parameters on combustion and emission characteristics of the HCCI diesel engines. Kiplimo *et al*. (2012) and Benajes *et al*. (2012) studied the impact of injection timing on performance and emission of an HCCI diesel engine. Results showed that an earlier injection timing resulted in higher soot, CO and HC emissions. This could be related to the fuel impingement on the piston surface and splashing to the crevices, which formed a rich-fuel region. However, the research results of Kim *et al*. (2008) and Kook *et al*. (2007) showed an opposite variation trends of soot emissions with the advance of the injection timing because of the lean in-cylinder mixture and low combustion temperature. The effects of the injection angle have been investigated by Mobasheri and Peng (2012), Fang *et al*. (2008) and Park *et al*. (2013) Results showed that limiting the injection angle was a useful approach to reduce the wall wetting phenomenon.

**Corresponding author.* e-mail: lxy@tju.edu.cn

However, whether the narrow injection angle could or couldn't improve the emission level was determined by the impingement target which directly influenced the in-cylinder mixture formation. Besides, the injection pressure had a significant effect on the combustion and emission characteristics of the HCCI diesel engines using early injection strategy. The higher injection pressure meant shorter injection duration and longer premixing time before the onset combustion. Moreover, the atomization of the fuel improved, which resulted in better air fuel mixing and less fuel-rich regions. However, the spray penetration length increased with higher injection pressure. This would cause serious wall wetting phenomenon and increased the wall film mass. This paradoxical effect finally decided the emission level of the HCCI diesel engines with different injection pressures (Park *et al*., 2012; Liu *et al*., 2015).

Based on the research results mentioned above, the combustion and emission characteristics of HCCI diesel engines using early injection strategy are directly affected by wall wetting characteristics. In this paper, the effects of the early injection parameters (injection timing, injection angle and injection pressure) on wall wetting characteristics of an HCCI diesel engine using early injection strategy have been numerically investigated. The variations of maximum wall film mass, evaporated wall film mass and residual wall film mass has been summarized. Because of the formation of over-rich fuel-air mixture in the near cylinder wall region due to the occurrence of wall wetting, the concept of MHI has been introduced to evaluate the homogeneity of fuel-air mixture in the wall wetting region. The variations of MHI value and mass fraction distribution of the regions with different equivalence range of the wall wetting region under various early injection parameters have been analyzed. In additions, the effects of the early injection parameters on the HC and CO emissions have also been discussed in order optimize the early injection parameters.

2. MODELING METHODOLOGY

2.1. Sub-models

The numerical model is carried out using commercially available three dimensional CFD code AVL Fire. The sub-models group including turbulence, spray breakup and evaporation and combustion models are presented in Table 1. The SKLE reduced reaction mechanism developed by Huang and Su (2005) for n-heptane with 44 species and 72 reactions is used to simulate diesel fuel combustion. In this study, the total emissions of aldehyde (formaldehyde, acetaldehyde and propionaldehyde), alkene (ethylene, propylene, 1,3-butadiene) and alkane (n-heptane) are considered as the engine HC emissions.

Table 1. Sub-model group.

Sub-model	Model name
Turbulence model	k-zeta-f model
Spray breakup model	Dukowicz model
Spray evaporation model	WAVE model
Combustion model	SKLE model

The spray-wall interaction model used in this study is provided by Zhang *et al*. (2014), which is developed with special emphasis on the conditions with high injection pressure and intermediate-to-high environment pressure.

The spray-wall interaction process has been distinguished between dry wall and wet wall conditions. The dry wall impingement regimes include deposition and splash, whereas the wet wall regimes consist of stick, rebound, spread, and splash. The regime transition thresholds of splash are determined based on Weber number of the impingement droplets as shown below:

$$We_{\mathrm{dry,splash}} = Oh^{0.4}(649 + 3.76R_{\mathrm{nd}}^{-0.63})$$

$$We_{\mathrm{wet,splash}} = \begin{cases} 450 & \delta \le 0.1 \\ 1.375.7\delta + 340 & 0.1 < \delta \le 1.0 \\ 1043.8 + 232.6\delta^{-1} - 1094.4\delta^{-2} + 1576.4\delta^{-3} & \delta > 1.0 \end{cases} \quad (1)$$

Where R_{nd} is defined as the ratio between the surface mean roughness (R) and the impingement droplet diameter (d_{b}). And δ is the dimensionless film thickness, which is defined as the ratio between the mean film thickness (h) and the impingement droplet diameter.

The mass ratio for the splash regime can be summarized as below considering the wall conditions,

$$\gamma_{\mathrm{m}} = \frac{m_{\mathrm{a}}}{m_{\mathrm{b}}} = \begin{cases} 0.8\{1 - exp[-3.17 \times 10^{-4}(K - K_{\mathrm{cr}})]\} & Dry\ wall \\ 0.2 + 0.9\varepsilon & Wet\ wall \end{cases} \quad (2)$$

Where $K = Oh^{-0.4}We$, K_{cr} = 10,396, and ε is a random number distributed uniformly in the interval (0,1).

The secondary droplets diameter for the splash regime are determined by using an updated log-normal distribution function as shown below,

$$f\left(\frac{d_{\mathrm{a}}}{d_{\mathrm{b}}}\right) = \frac{\sqrt{3}}{\sqrt{\pi}(d_{\mathrm{a}}/d_{\mathrm{b}})} exp\left\{-3\left[ln\left(\frac{d_{\mathrm{a}}}{d_{\mathrm{b}}}\right) - \frac{1}{6} - ln\left(\frac{d_{\mathrm{m}}}{d_{\mathrm{b}}}\right)\right]\right\} \quad (3)$$

Where d_{a} is the diameter of secondary droplet. The value of $d_{\mathrm{m}}/d_{\mathrm{b}}$ is a function of $\boldsymbol{K'}$ ($K' = WeRe^{0.5}$) and is calculated by

$$\frac{d_{\mathrm{m}}}{d_{\mathrm{b}}} = \max(19.86K'^{-0.5}, 0.05) \quad (4)$$

Mean secondary droplet normal and tangential velocities are scaled with impingement droplet normal and tangential velocities, respectively, while the widths of both the secondary droplet normal and tangential velocity distributions are scaled approximately with impingement

droplet normal velocity.

$$\mathbf{V}_a = V_{an}\boldsymbol{n} + V_{at}(\cos\psi\boldsymbol{e}_t + \sin\psi\boldsymbol{e}_p) \quad (5)$$

Where $\boldsymbol{n}$ is the unit normal to the wall surface, $\boldsymbol{e}_t$ is the unit vector tangent to the surface and in the plane of $\boldsymbol{n}$; $\boldsymbol{e}_p = \boldsymbol{n} \times \boldsymbol{e}_t$. V_{an} is the normal component of the secondary droplet velocity while V_{at} is the tangential component. The quantity V_{an} is the normal component and is chosen from the Nukiyama-Tanasawa distribution:

$$f(V_{an}) = \frac{4}{\sqrt{\pi}}\frac{(V_{an})^2}{V_{a,max}^3} exp\left[-\left(\frac{V_{an}}{V_{a,max}}\right)^2\right] \quad (6)$$

Where $V_{a,max} = 0.3V_{bn}$ and V_{bn} is the impingement droplet normal velocity.

The quantity V_{at} is calculated by the V_{bt} which is the impingement droplet tangential velocity as follow:

$$V_{at} = \xi V_{bt} \quad (7)$$

Where ξ is the friction coefficient. In this study, the friction coefficient is 0.95. Finally, the azimuth angle ψ is defined as the angle that the tangential velocity makes with the vector $\boldsymbol{e}_t$ in the plane of the wall. Ψ lies in the interval (0, π) and is statistically calculated by the distribution suggested by Naber and Reitz (1988) as:

$$\psi = -\frac{\pi}{\beta} ln[1 - k(1 - e^{-\beta})] \quad (8)$$

Where k is another random number distributed uniformly in the interval (0,1), and β is a parameter related to the impact angle α by

$$\sin\alpha = \frac{e^{\beta}+1}{e^{\beta}-1}\frac{\beta^2}{\beta^2+\pi^2} \quad (9)$$

And α is the angle between the impingement droplet velocity and the wall normal $\boldsymbol{n}$.

2.2. Calculation Meshes and Initial Conditions

The specifications of the diesel engine used for modeling are shown in Table 1 and the fuel injection parameters are shown in Table 2. The operation conditions for this study is fixed at engine speed of 2,000 rpm.

The calculation meshes used in this study is a 1/6 sector model of one fuel spray based on the assumption of cyclic symmetry which consists about 71,280 cells, as shown in Figure 1. Calculations are carried out on the closed system from intake valve close at 132 BTDC (before top dead center) to exhaust valve open at 114 ATDC (after top dead center). The initial conditions contain charge pressure (2.01 bar), charge temperature (340 K), piston head temperature (550 K), cylinder head temperature (550 K) and cylinder wall temperature (475 K).

Table 2. Engine specification (YN4100QBZL).

Parameter	Value
Type	4 cylinder inline, naturally aspirated
Bore × Stroke	100 × 105 mm
Compression ratio	17.5 : 1
Swirl ratio	3.4
Type of combustion chamber	ω type

Table 3. Injection system specification.

Parameters	Value
Mass of fuel injected	6 mg
Spray angle	160-degree
Spray cone angle	8-degree
Holes no./Nozzle diam.	6/0.24 mm
Start of the injection timing	10° BTDC

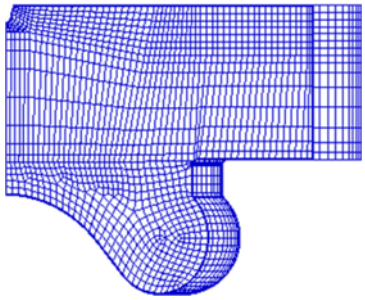

Figure 1. Calculation grid used in this study.

2.3. Model Validation

For model validation, Figure 2 (a) shows the comparison of the measured and calculated cylinder pressure and heat release rate curves. The difference between the measured and calculated was mainly attributed to the difference physical and chemical properties between the diesel and n-heptane. In addition, the heat transfer loss was not considered in the calculation process, which also resulted the higher heat release rate of the calculated result. Figure 2 (b) shows the measured and calculated engine-out HC and CO emissions. The lower HC and CO emissions of the calculated results than the measured results was mainly due to the lack of the long chain hydrocarbon, cycloalkane, and aromatic hydrocarbon for n-heptane compared with diesel, which were the main source of the formation of HC and CO emissions. In general, the calculated results shown in these figures capture the features of the measured results well.

2.4. Modeling Conditions

In this paper, only single early injection strategy has been discussed, and the parameters of the early injection

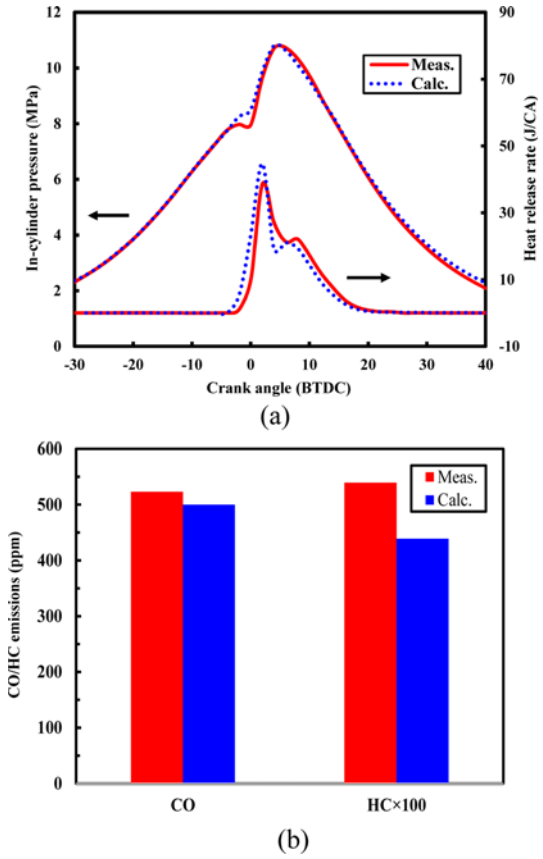

Figure 2. Comparison of calc. and meas. cylinder pressure and heat release rate (a) and emission characteristics (b).

Table 4. Modeling conditions.

Varying injection timing (Injection angle: 160-degree, Injection pressure: 100 MPa)					
Injection timing (BTDC)	40	50	**60**	70	80
Varying injection angle (Injection timing: 40 BTDC, Injection pressure: 100 MPa)					
Injection angle (degree)	80	100	120	140	**160**
Varying injection pressure (Injection timing: 40 BTDC, Injection angle: 160-degree)					
Injection pressure (MPa)	60	80	**100**	120	160

parameters include the injection timing, injection angle and injection pressure as summarized in Table 4. A set of conditions in which the injection timing, injection angle and injection pressure are 60 BTDC, 160-degree and 100 MPa, respectively, is used as a reference.

3. RESULTS AND DISCUSSION

3.1. Effects of Early Injection Parameters on Wall Film Mass

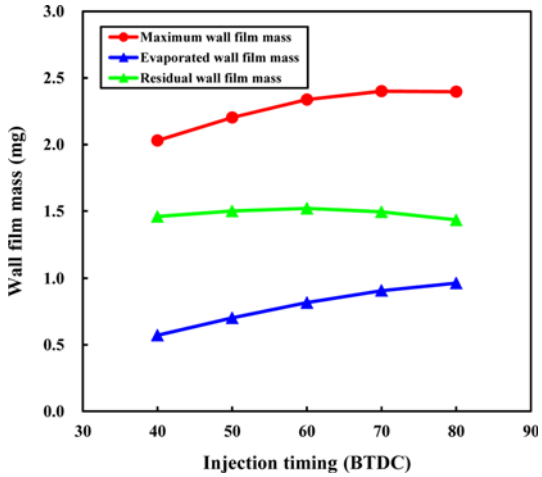

Figure 3. Variations of the wall film mass according to different injection timings.

In this section, the variations of the maximum wall film mass, evaporated wall film mass and the residual wall film mass have been discussed. The maximum wall film mass is defined as the maximum mass of wall film formed during the early injection period. The evaporated wall film mass is the total evaporated mass of the wall film before the SOI (start of the ignition), and SOI is defined as the crank angle when the accumulated heat release reached 10 % of the total heat release. The residual wall film mass is the difference between the maximum wall film mass and evaporated wall film mass. In addition, for all the modeling conditions, the timing of the SOI are located between 20 ~ 10 BTDC, so in this paper, the wall film characteristics under the crank angle of 20 BTDC have been discussed.

As shown in the Figure 3, with the advance of the injection timing, the maximum wall film mass continuously increased however the increasing rate slowed down. This was because the lower in-cylinder density and temperature at the earlier injection timing shortened the spray penetration time and weakened the spray atomization resulting in more injected fuel impinging with the cylinder wall and increasing the maximum wall film mass. In addition, the evaporated wall film mass linearly increased with the advance of the injection timing due to the increase of the wall film evaporation time. These two reasons resulted a first increased then decreased variation trend of the residual wall film mass and the highest residual wall film mass was obtained when the injection timing was 60 BTDC.

As shown in the Figure 4, with the increase of the injection pressure, the maximum wall film mass decreased first then remained at a constant level. This was mainly attributed into the enhancement of the spray atomization. With the increase of the injection pressure resulting in more fuel atomized in the penetration duration and less fuel impinged against the wall. However, shortening the spray penetration duration due to the high injection pressure

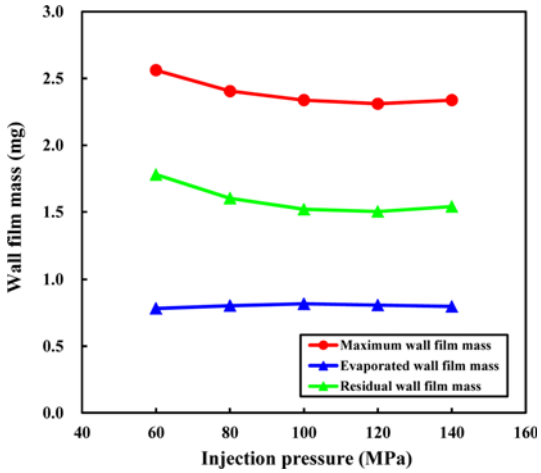

Figure 4. Variations of the wall film mass according to different injection pressures.

weakened wall film mass reduction. The evaporated wall film mass changed a little, which resulted the variation trend of the residual wall film mass was the same with the maximum wall film mass's.

As shown in the Figure 5, with the decrease of the injection angle, the maximum wall film mass decreased. This was because that the spray penetration distance between the nozzle and the cylinder wall prolonged as the decrease of the injection angle and more injected fuel was atomized in the penetration duration. For the variation of evaporated wall film mass, with the decrease of the injection angle, the evaporated wall film mass first decreased slightly due to the shorter evaporation duration. However, when the injection angle decreased to 120 degree, the variation showed a step increasing trend, which was attributed to the change of the impingement target from cylinder wall to piston head or piston bowl. Due to the higher surface temperature of piston head and piston bowl than the cylinder wall, the wall film evaporation enhanced obviously resulting in the step increase of the evaporated wall film mass. The residual wall film mass decreased linearly with the decrease of the injection angle, and decreased sharply when the injection angle decreased to 120 degree. In addition, no residual wall film was observed when the injection angle was 80 degree.

3.2. Effects of Early Injection Parameters on Mixture Formation

Figure 6 represented the variations of the fuel-air distribution of the in-cylinder mixture after the occurrence of early injection. After the spray impinged with the cylinder wall, the fuel-air mixture formed along the upwards and downwards direction of the cylinder wall. On one hand, the upward mixture spread to the clearance region-the junction region of cylinder wall and cylinder head. On the other hand, the downward mixture developed along the cylinder wall and also formed the over-rich regions near the cylinder wall.

The over-rich mixture in the near wall region due to the occurrence of wall wetting will cause the incomplete combustion and excessive HC and CO emissions. Moreover, the combustion of the over-rich mixture in the near wall region also raises the temperature, which increases the heat transfer loss through the cylinder wall. Because of this, it is considered necessary to investigate the fuel-air mixture formation in the near wall region. In this paper, the near wall region is defined as wall wetting regions as shown in Figure 7.

In addition, In order to evaluate the homogeneity of the fuel-air mixture, the concept of a Mixture Homogenous Index (MHI) is introduced.

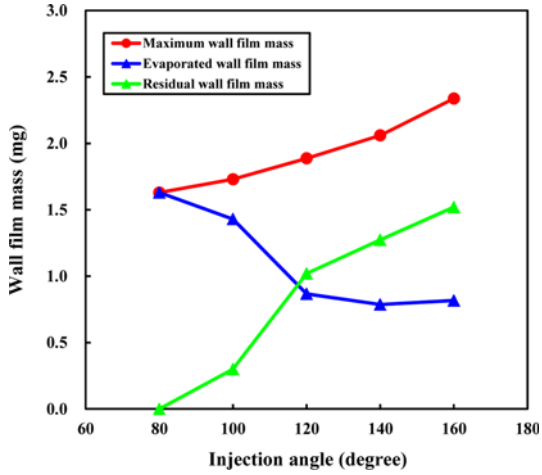

Figure 5. Variations of the wall film mass according to different injection angles.

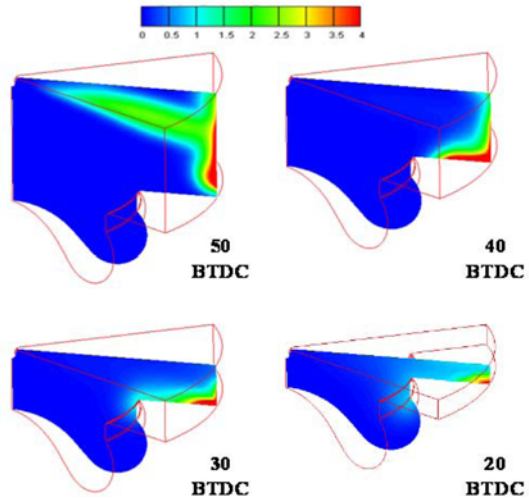

Figure 6. In-cylinder equivalence distribution according to the crank angle.

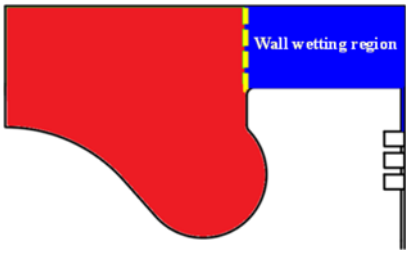

Figure 7. Definition of the wall wetting region.

MHI value is calculated as:

$$MHI = \frac{SD}{\overline{\varphi}} \tag{10}$$

Where, the mean equivalence ratio ($\overline{\varphi}$) of the in-cylinder fuel-air mixture is calculated as:

$$\overline{\varphi} = \frac{\Sigma_i^{n_{cell}} \varphi_i \delta m_i}{\Sigma_i^{n_{cell}} \delta m_i} \tag{11}$$

n_{cell} is the total number of the cells, φ_i is the equivalence ratio of each cell, and δm_i is the mass of each cell.

Where, the standard deviation (SD) of the equivalence ratio in the computational domain is defined as

$$SD = \sqrt{\frac{\Sigma_i^{n_{cell}} (\varphi_i - \overline{\varphi})^2 \delta m_i}{\Sigma_i^{n_{cell}} \delta m_i}} \tag{12}$$

MHI is an indicator of the mixture homogeneity: lower values of MHI represents more homogeneous mixtures.

The variations of the MHI and the mass fraction distribution of the regions with different equivalence range of the wall wetting region when varying the early injection parameters have been analyzed below. The mixture formation investigation is also focused on the crank angle of 20 BTDC.

With the advance of the injection timing, the variations of the MHI value of the wall wetting region showed a continuous decreasing trend as shown in Figure 8 (a), however, when the injection timing advanced to 70 BTDC, the decreasing rate slowed down. This was because that the earlier injection timing prolonged the fuel-air mixing time, which was favor for the homogeneous mixture formation. While, the evaporated wall film mass also increased, this was against to the homogeneous mixture formation and slowed down the decreasing rate.

As shown in Figure 8 (b), as the advance of the injection timing, the mass fraction of the region with low equivalence ratio (φ < 0.5) first decreased then increased. This was because that when the injection timing was closed to TDC (60 ~ 40 BTDC), the mixing time was not long enough for the whole wall wetting region filled by the fuel-air mixture resulting in the increase of the mass fraction. Further advancing the injection timing (80 ~ 60 BTDC), the overall equivalence ratio decreased due to the longer mixing time

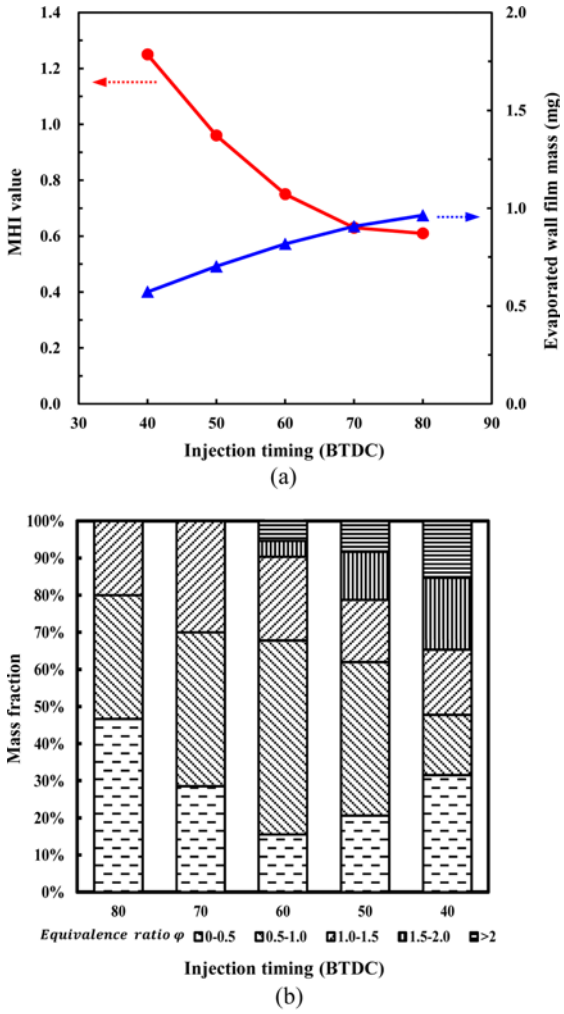

Figure 8. (a) Variations of MHI value and evaporated wall film mass; (b) Mass fraction distribution of the regions with different equivalence range according to different injection timings.

resulting in the increasing the mass fraction again. The mass fraction of the over-rich region (φ > 2.0) decreased gradually and disappeared after the injection timing was earlier than 60 BTDC.

The variation of the MHI value of the conditions with different injection pressure was shown in Figure 9 (a). With the increase of the injection pressure, the MHI value decreased. Because of the evaporated film mass changed little according to the variation of the injection pressure, the decreasing trend of the MHI value was mainly attributed to better spray atomization and longer mixing time. In additions, it was worth noting that the amplitude of variation of the MHI value with different injection pressure was smaller than the conditions with different injection timing.

With the increase of the injection pressure, the mass fraction of the region with low equivalence ratio also

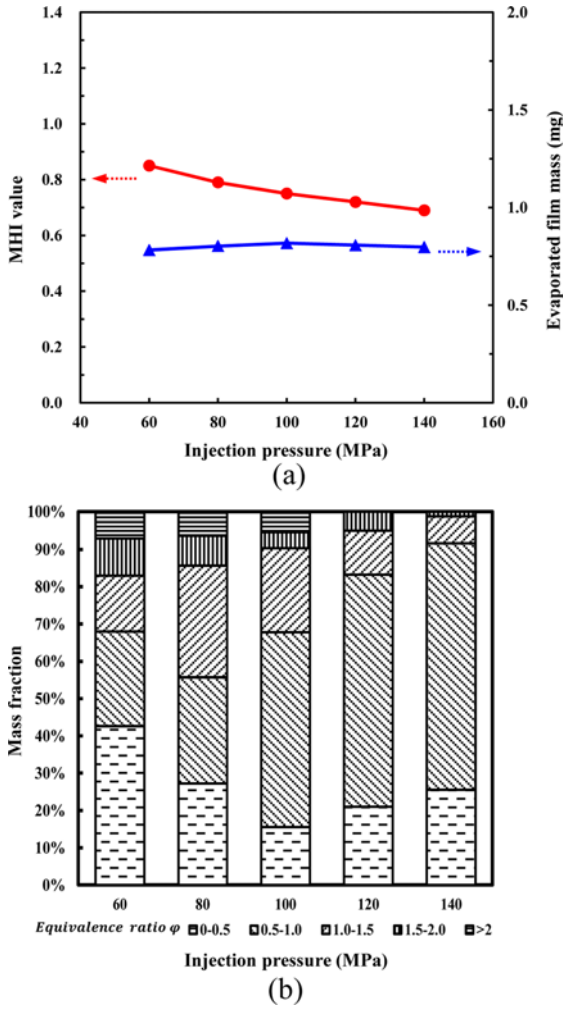

Figure 9. (a) Variations of MHI value and evaporated wall film mass; (b) Mass fraction distribution of the regions with different equivalence range according to different injection pressures.

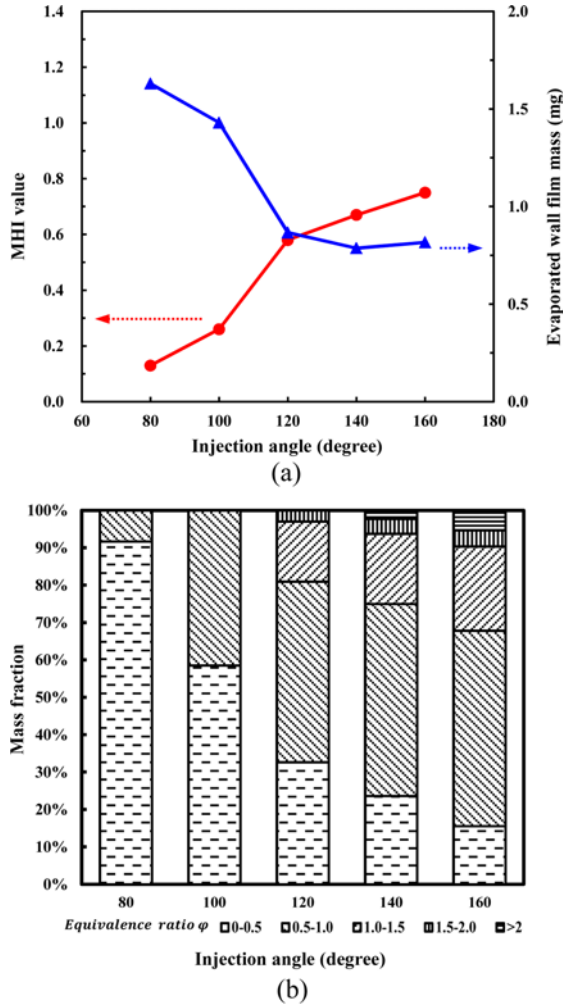

Figure 10. (a) Variations of MHI value and evaporated wall film mass; (b) Mass fraction distribution of the regions with different equivalence range according to different injection angles.

showed a first decreasing then increasing trend. This was because that for the conditions with lower injection pressure (60 ~ 100 MPa), increasing the injection pressure decreased the wall film mass and more injected fuel participated in fuel-air mixture formation resulting in a higher equivalence ratio. Further increasing the injection pressure (100 ~ 140 MPa), the improvement of the entrainment between the fuel and air again decreased the equivalence ratio and increase the mass fraction of the region with low equivalence ratio. Mass fraction with high equivalence ratio ($1.5 < \varphi < 2.0$) decreased obviously and over-rich region became zero when the injection pressure exceeded 120MPa as shown in Figure 9 (b).

As decreasing the injection angle, the MHI value of the wall wetting region showed step decreasing trend, and the step point took place when the injection angle was 120-degree as shown in Figure 10 (a). This was because of the variation of impingement target from the cylinder wall to the piston bowl. On one hand, the increase surface temperature of the piston bowl enhanced the mixture formation. On the other hand the air flow movement also strengthened which was also beneficial for the formation of the homogenous mixture.

As shown in Figure 10 (b), the mass fraction of the region with low equivalence ratio increased, while the mass fraction of the region with high equivalence ratio decreased as the decrease of the injection angle. Moreover, the over-rich region disappeared when injection angle was narrowed to 100 degree.

3.3. Effects of Early Injection Parameters on HC and CO Emissions

Figure 11 (a) shows the effect of injection timing on HC and CO emissions. As the advance of the injection timing,

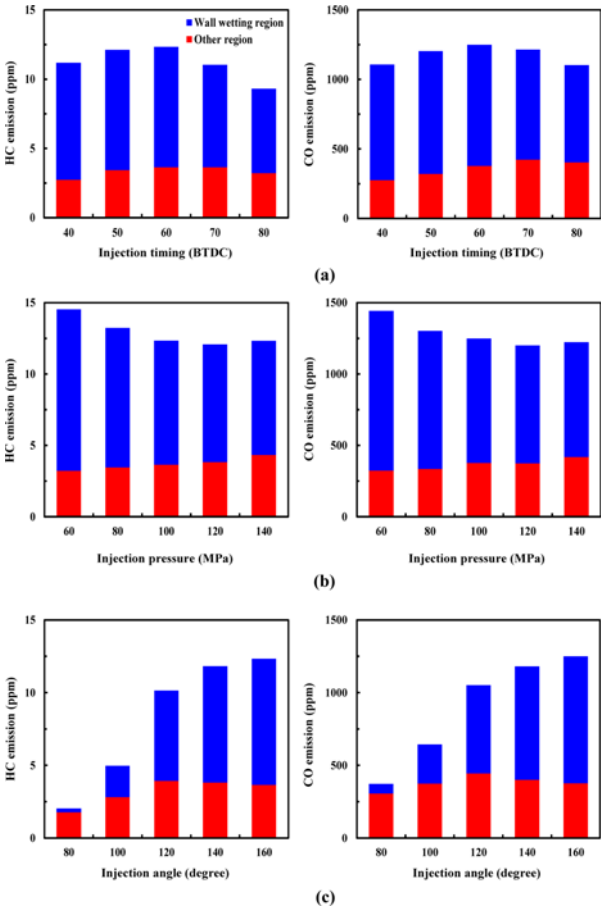

Figure 11. Effects of the early injection parameters on HC and CO emissions.

the variation trends of both HC and CO emissions showed a first increasing then decreasing trend. In addition, it could be seen that the HC and CO emissions in the wall wetting region was the main source to the overall emissions, that was the HC and CO emissions in the wall wetting region mainly controlled the overall HC and CO emissions.

Similar to the conditions with different the injection timings, wall wetting region also had the greatest contribution on the HC and CO emissions when varying the injection pressure as shown in Figure 11 (b). As the increase of the injection pressure, both HC and CO emissions decreased and slightly increased and obtained the lowest value when the injection pressure was 120 MPa.

Figure 11 (c) shows the effect of injection angle on HC and CO emissions. With the decrease of the injection angle, both HC and CO first slightly decreased. Further decreasing the injection angle over 120 degree, the HC and CO emissions decreased sharply and obtained the lowest values when the injection angle was 80 degree. This was because the variation of the impingement target. The impingement target changed from the cylinder wall to the piston head or piston bowl as the decrease of the injection angle, and the surface temperature of the piston head or piston bowl was much higher than the cylinder wall which enhanced the wall film evaporation and decreased the residual wall film mass. Moreover, the lowest HC and CO emissions for the condition of 80 degree was also attributed that the impingement target was the piston bowl lip, which also enhanced the secondary atomization process and promoted the mixture formation.

In addition, the wall wetting region also had the greatest contribution on the HC and CO emissions for the conditions with larger injection angle, however, HC and CO emissions in the wall wetting region decreased obviously for the narrow injection angle conditions, and even could be ignored for the 80 degree condition. This also indicated that the variation of the overall HC and CO emissions was still mainly controlled by the HC and CO emissions in the wall wetting region.

3.4. Relationships between Wall Film Characteristics and HC and CO Emissions

As discussed that above, the variations of overall HC and CO emissions were attributed to the HC and CO emissions variations in the wall wetting region. The HC and CO emissions in the wall wetting region was mainly attributed to two impact factors. One was the homogeneity of the

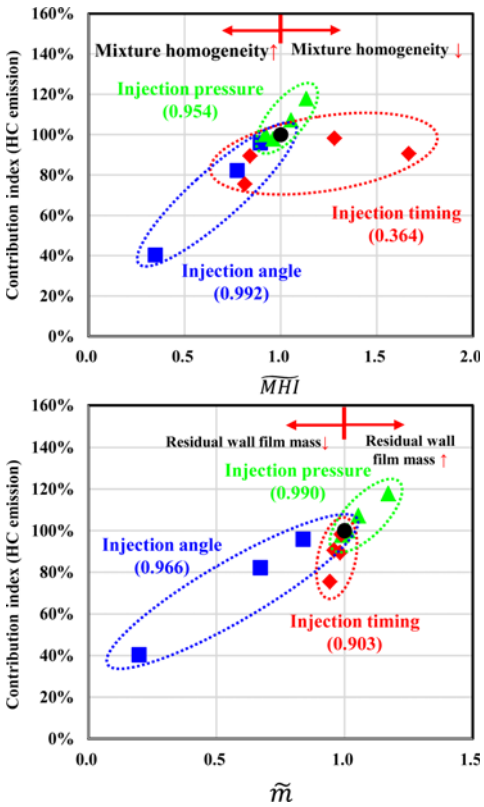

Figure 12. Contribution of the impact factors of mixture homogeneity and residual wall film mass on the HC emissions.

fuel-air mixture in the wall wetting region, the other was the residual wall film mass. More homogenous fuel-air mixture and less residual wall film mass was contributed to the decrease of the HC and CO emissions. In order to separate and evaluate the effects of these two factors on the HC and CO emissions in the wall wetting region, two dimensionless numbers were introduced. These were defined as below:

$$\widetilde{MHI} = \frac{MHI_i}{MHI_0}, \ \tilde{m} = \frac{m_i}{m_{0_i}} \tag{13}$$

where the subscript i represented each experiment condition and the subscript 0 represented the reference case. MHI was the fuel-air mixture homogeneity value, m was the residual wall film mass.

A correlation analysis was performed, and the correlation coefficients between the HC and CO emissions and the two impact factors were obtained.

As shown in Figure 12, when varying the injection timing, the effect of the residual wall film mass on the HC emissions variation was greater than the effect of the mixture homogeneity, which indicated that the variation of the residual wall film mass was the main impact factor. However, for the conditions with different injection angle and injection pressure, the variation of the HC emissions was combined affected by these two impact factors and were in the same level.

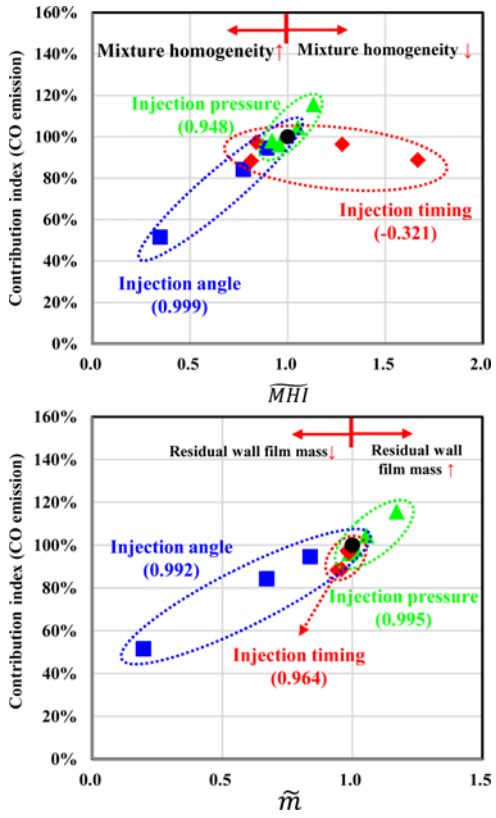

Figure 13. Contribution of the impact factors of mixture homogeneity and residual wall film mass on the CO emissions.

Similar to the HC variation, the variation of the residual wall film mass was the main impact factor on the CO emissions variation when varying the injection timing, and the effect of the mixture homogeneity was even masked by the effect of residual wall film mass as shown in Figure 13. The variation of the CO emissions was also combined affected by these two impact factors for the conditions with different injection pressure and angle.

4. CONCLUSION

In this study, the effects of the early injection parameters (injection timing, injection angle and injection pressure) on wall wetting characteristics of an HCCI diesel engine using early injection strategy have been numerically investigated. The following conclusions can be drawn from this work:

(1) With the advance of the injection timing, the variation of residual wall film mass showed a first increasing then decreasing trend. With the increase of the injection pressure, the residual wall film mass decreased first then remained at a constant value. Decreasing the injection angle smaller than 120 degree, the residual wall film mass decreased sharply.

(2) The homogeneity of the fuel-air mixture in the wall wetting region could be improved by advancing the injection timing, increasing the injection pressure and decreasing the injection angle. In addition, when the impingement target was the piston bowl lip, the fuel-air mixing could be also enhanced.

(3) For HCCI diesel engine, with the advance of the injection timing, the variations of HC and CO emissions showed a first increasing then decreasing trend, and obtained the highest value when the injection timing of 60 BTDC. With the increase of the injection pressure, it showed a first decreasing then increasing trend, and obtained the lowest value when the injection pressure was 120 MPa. With the decrease of the injection angle, the HC and CO emissions showed a step decreasing when the injection angle was smaller than 120-degree. In addition, the variations of overall HC and CO emissions were attributed to the HC and CO emissions variations in the wall wetting region.

(4) The HC and CO emissions in the wall wetting region was mainly attributed to impact factors of the homogeneity of the fuel-air mixture in the wall wetting region and the residual wall film mass. More homogenous fuel-air mixture and less residual wall film mass were contributed to the decrease of the HC and CO emissions. When varying the injection timing the effect of the residual wall film mass on the HC and CO emissions variations was greater than the effect of the mixture homogeneity. For the conditions with different injection pressure and injection angle, the

variation of the HC and CO emissions were combined affected by these two impact factors and were in the same level.

(5) In order to decrease the HC and CO emission caused by wall wetting as low as possible, it was better to increase the injection pressure, advance the injection timing. And the most effective method was to narrow the injection angle, In addition, the impingement target should be considered for choosing the injection timing and injection angle, and the impingement target of the piston bowl lip was recommended due to the enhancement of the atomization and the higher surface temperature.

ACKNOWLEDGEMENT–This work was supported by National Natural Science Foundation of China (No. 51376136 and No. 51406132) and Natural Science Foundation of Tianjin (No. 14JCYBJC21300). We also wish to thank AVL LIST GmbH for their support by providing the AVL-AST software FIRE.

REFERENCES

Benajes, J., García-Oliver, J. M., Novella, R. and Kolodziej, C. (2012). Increased particle emissions from early fuel injection timing diesel low temperature combustion. *Fuel*, **94**, 184–190.

Berggren, C. and Magnusson, T. (2012). Reducing automotive emissions The potentials of combustion engine technologies and the power of policy. *Energy Policy*, **41**, 636–643.

Fang, T., Coverdill, R. E., Chia-fon, F. L. and White, R. A. (2008). Effects of injection angles on combustion processes using multiple injection strategies in an HSDI diesel engine. *Fuel* **87**, **15**, 3232–3239.

Huang, H. and Su, W. (2005). A new reduced chemical kinetic model of N-Heptane combustion for HCCI engine simulations. *Trans. Csice* **23**, **1**, 42–51.

Jia, M., Peng, Z., Xie, M. and Stobart, R. (2008). Evaluation of spray/wall interaction models under the conditions related to diesel HCCI engines. *SAE Paper No*. 2008-01-1632.

Kim, H., Kim, Y. and Lee, K. (2008). A study of the characteristics of mixture formation and combustion in a PCCI engine using an early multiple injection strategy. *Energy and Fuels* **22**, **3**, 1542–1548.

Kiplimo, R., Tomita, E., Kawahara, N. and Yokobe, S. (2012). Effects of spray impingement, injection parameters, and EGR on the combustion and emission characteristics of a PCCI diesel engine. *Applied Thermal Engineering*, **37**, 165–175.

Kitasei, T., Yamada, J., Shoji, T., Shiino, S. and Mori, K. (2008). Influence of the different fuel spray wall impingement angles on smoke emission in a DI-diesel engine. *SAE Paper No*. 2008-01-1791.

Kook, S., Park, S. and Bae, C. (2007). Influence of early fuel injection timings on premixing and combustion in a diesel engine. *Energy and Fuels* **22**, **1**, 331–337.

Liu, H., Ma, S., Zhang, Z., Zheng, Z. and Yao, M. (2015). Study of the control strategies on soot reduction under early-injection conditions on a diesel engine. *Fuel*, **139**, 472–481.

Mobasheri, R. and Peng, Z. (2012). A computational investigation into the effects of included spray angle on heavy-duty diesel engine operating parameters. *SAE Paper No*. 2012-01-1714.

Musculus, M. P. B., Miles, P. C. and Pickett, L. M. (2013). Conceptual models for partially premixed low-temperature diesel combustion. *Progress in Energy and Combustion Science* **39**, **2**, 246–283.

Naber, J. and Reitz, R. (1988). Modeling engine spray/wall impingement, *SAE Paper No*. 880107.

Noguchi, M., Tanaka, Y., Tanaka, T. and Takeuchi, Y. (1979). A study on gasoline engine combustion by observation of intermediate reactive products during combustion. *SAE Paper No*. 790840.

Onishi, S., Jo, S. H., Shoda, K., Jo, P. D. and Kato, S. (1979). Active thermo-atmosphere combustion (ATAC) – A new combustion process for internal combustion engines. *SAE Paper No*. 790501.

Park, S. H., Cha, J., Kim, H. J. and Lee, C. S. (2012). Effect of early injection strategy on spray atomization and emission reduction characteristics in bioethanol blended diesel fueled engine. *Energy* **39**, **1**, 375–387.

Park, S. H., Yoon, S. H. and Lee, C. S. (2013). HC and CO emissions reduction by early injection strategy in a bioethanol blended diesel-fueled engine with a narrow angle injection system. *Applied Energy*, **107**, 81–88.

Yao, M., Zheng, Z. and Liu, H. (2009). Progress and recent trends in homogeneous charge compression ignition (HCCI) engines. *Progress in Energy and Combustion Science* **35**, **5**, 398–437.

Yu, H., Guo, Y., Li, D., Liang, X., Shu, G., Wang, Y., Wang, X. and Dong, L. (2015). Numerical investigation of the effect of spray cone angle on mixture formation and CO/Soot emissions in an early injection HCCI diesel engine. *SAE Paper No*. 2015-01-1070.

Zhang, Y., Jia, M., Liu, H., Xie, M., Wang, T. and Zhou, L. (2014). Development of a new spray/wall interaction model for diesel spray under PCCI-engine relevant conditions. *Atomization and Sprays* **24**, **1**, 41–80.